

## Classical description of electron structure near a positive ion

Bernard Talin and Annette Calisti

*Université de Provence, CNRS UMR 6633, Centre Saint Jérôme, 13397 Marseille Cedex 20, France*

James Dufty

*Department of Physics, University of Florida, Gainesville, Florida 32611*

(Received 8 January 2002; published 2 May 2002)

A single positive ion is imbedded in an electron gas with overall charge neutrality. A classical statistical mechanics is considered using an electron-ion Coulomb potential regularized at distances within the de Broglie length. The electron charge density and electric field distribution at the ion are studied as a function of ion-electron coupling using molecular dynamics simulation and theoretical models. Agreement between theory and simulation is quite good in general, although differences are observed for very strong ion-electron coupling due to the enhanced importance of close electron-ion configurations.

DOI: 10.1103/PhysRevE.65.056406

PACS number(s): 52.65.Yy, 52.25.Vy, 05.10.-a

### I. INTRODUCTION

Systems comprised of charged particles are of fundamental interest for many fields of physics and chemistry. For fully ionized systems the dominant effects of electrons often can be captured through their screening of the ion-ion interaction potential. This is essentially a Born-Oppenheimer approximation that is at the core of many approaches in statistical mechanics and condensed matter. Typically the motion of ions is semiclassical due to their mass and many tools of classical statistical mechanics are available to study their structure and dynamics. For example, a hydrogen plasma is modeled in this way by a classical one-component plasma of ions (OCP) interacting via an electron screened ion-ion potential. During the past 30 years significant progress has been made in the field of classical plasma physics to understand the properties of such ionic plasmas [1]. An important role in these studies has been played by molecular dynamics (MD) simulation, both to provide benchmarks for approximate theoretical methods and to explore the parameter space beyond available theories. More recently, attention has focused on improved descriptions of electron-ion plasmas by including the structure and dynamics for the electrons as well as the ions. A number of methods are available to describe the structural features of electrons, such as density functional, quantum Monte Carlo, and Car-Parrinello simulations. Typically, these have been developed for low temperatures and treat well the quantum effects that dominate below the electron Fermi temperature. Their application at higher temperatures and extensions to time dependent properties are somewhat more phenomenological. At higher temperatures, it is tempting to apply semiclassical methods for both the electrons and ions. This is sensible for systems that have a classical limit (e.g., jellium, the quantum OCP for electrons). However, the electron-ion plasma does not have a simple classical limit at the microscopic level due to the unbounded attractive electron-ion Coulomb interaction. The thermodynamic stability of the system requires some quantum features for the short distance interaction of opposite sign charges. For this and other reasons described below, the approaches used for classical plasmas do not extend in a straightforward

way to systems of electrons and positive ions (e.g., hydrogen). In particular the most powerful approach, MD, is strictly an implementation of classical mechanics and its utility for electron-ion systems is limited in principle.

Nevertheless, it is known that some properties of inherently quantum systems have classical or near classical limits for appropriate state conditions. For example, the equation of state of a classical hydrogen plasma approaches that of the Debye-Hückel theory, independent of Planck's constant, for sufficiently low density and high temperature [2]. This suggests that semiclassical methods may be appropriate to explore electron structure and dynamics in some limited domain of state conditions. One approach is to postulate a classical mechanics with the most important quantum effects represented through modifications of the interparticle potentials. These effects can be discovered by calculation of the two particle Slater sums, which become Boltzmann factors in terms of the classical pair potential whenever a classical limit exists, but otherwise they define modifications of the pair potential due to indelible quantum effects [3–5]. Typically, the classical Coulomb potential is modified in this way at distances shorter than the de Broglie wavelength to remove the singularity. Other methods not tied to the equilibrium state are available to define regularized potentials (e.g., wave packet MD [6]), but qualitatively all are similar. The basic assumption is that a many-body Hamiltonian constructed with these potentials defines a classical system of electrons and ions whose properties “resemble” the underlying quantum system in some portions of phase space. Alternatively, it can be viewed as a model classical system of particles with both attractive and repulsive interactions whose properties are of interest to discover for purely academic reasons.

In this context, most interest to date has focused on MD simulation of a classical representation of dense hydrogen [7–9], or related equal mass “electron-positron” models [10]. The objective here is somewhat different. A much simpler system consisting of a single positive ion embedded in a fluid of electrons (jellium) with overall charge neutrality is considered. This is a well-studied model for the case of a proton in jellium for conditions of strong electron degeneracy. The work here focuses on nondegenerate electrons and

impurities of higher charge number  $Z$  to force strong electron-ion coupling. The applicability of MD and certain standard theoretical methods of classical plasma physics is explored for calculating the electron charge distribution near the ion and the distribution of electric fields at the ion. A discussion of related dynamical properties (e.g., field autocorrelation function, stopping power, diffusion) will be presented elsewhere. Partial results of this study have been reported in Refs. [11–13]. For this simple impurity system there are only three dimensionless parameters: the charge number of the ion  $Z$ , the electron-electron coupling constant  $\Gamma$ , and the de Broglie wavelength relative to the interelectron distance  $\delta$  (defined more precisely in the following section). The electron-ion coupling is measured by the value of the regularized ion-electron potential at the origin,  $\sigma = Z\Gamma/\delta$ . In the following section it is shown that the application of semiclassical methods requires  $\sigma > 1$  and  $\delta < 1$ . Molecular dynamics results are reported here for two density temperature conditions,  $n = 2.5 \times 10^{22} \text{ cm}^{-3}$ ,  $T = 7.9 \times 10^5 \text{ K}$  and  $n = 3.2 \times 10^{18} \text{ cm}^{-3}$ ,  $T = 7.9 \times 10^3 \text{ K}$ . In both cases the electron-electron coupling is weak,  $\Gamma = 0.1$  and  $0.5$ , respectively. However, the electron-ion coupling can be strong, with  $\sigma = 0.25Z$  and  $\sigma = 2.5Z$ , respectively. Specifically the values  $\sigma = 2, 5, 7.5$ , and  $10$  are studied using charge numbers in the range  $Z \leq 40$ . The weak electron coupling was chosen to minimize any complications regarding the many-body physics for the electrons, which comprise a classical system in the absence of the impurity ion for these conditions. Thus the classical methods are being tested solely with respect to their ability to describe the electron-ion interaction.

There are two distinct issues in the application of classical methods to electron-ion systems. First is the accuracy of the model classical system in representing the actual quantum system of interest. Second is the accuracy of existing classical methods to describe the model classical system. The first issue is considered here only qualitatively in the following section in discussing the parameter space considered. Instead, attention is focused on the second issue regarding the statistical mechanics of the model classical system. A direct translation of standard methods to this system is subject to question because the dominant configurations now include short distances, which are irrelevant for the more usual repulsive interactions at short range. The closest analog is a system of charged hard spheres with both positive and negative charges representing electrolytes [5]. The short range attraction necessitates changes in implementation of the MD simulations and limitations on the range of validity for certain theoretical approximations. The theoretical models considered here are based on the hypernetted chain approximation (HNC) integral equation for the electron-electron and electron-ion charge densities. Properties of the electron electric field at the ion (covariance and microfield distribution) are obtained from approximations that are determined from these charge densities. The microfield distribution and its nearest neighbor approximation are calculated from MD, the Baranger-Moser (BM) approximation [14], and its extension to strong coupling APEX [15].

The context of the calculations presented here is discussed in the following section to clarify the relevance for real sys-

tems and to distinguish the components that are less practical explorations of extreme conditions for the classical model. Also in this section the MD simulation method and theoretical models are discussed briefly, emphasizing any points of concern associated with the attractive potential. In Sec. III, the electron charge density results are presented and discussed. The electric field covariance and electron microfield are considered in Sec. IV. Finally, a number of conclusions are drawn in the last section.

## II. THEORY AND SIMULATION

The system considered in this paper consists of  $N_e$  electrons with charge  $-e$ , an infinitely massive positive ion with charge  $Ze$  placed at the origin, and a rigid uniform positive background for overall charge neutrality. The uniform density of the background is therefore related to the electron density  $n_e = N_e/\Omega$  by

$$n = n_e - \frac{Z}{\Omega} = n_e \left( 1 - \frac{Z}{N_e} \right), \quad (1)$$

where  $\Omega$  is the volume. The electron-electron and electron-background interactions are taken to be Coulomb while the electron-ion interactions occur via a regularized Coulomb potential  $V(r)$ . The Hamiltonian is

$$H = \sum_{i=1}^{N_e} \frac{p_i^2}{2m_e} + \sum_{i \neq j}^{N_e} \frac{e^2}{|\mathbf{r}_i - \mathbf{r}_j|} + \sum_i^{N_e} Ze^2 V(r_i) - \sum_i^{N_e} \int_{\Omega} d\mathbf{r} \frac{1}{|\mathbf{r}_i - \mathbf{r}|} n e^2 + U_0. \quad (2)$$

Here  $\mathbf{p}_i$  is the momentum of the  $i$ th electron and  $m_e$  is the electron mass. Also,  $U_0$  is independent of the electron coordinates and represents the background self-energy contributions. This can be set equal to zero without loss of generality. The regularized electron-ion potential is chosen to be

$$V(r) = -\frac{Ze^2}{r} (1 - e^{-r/\delta}), \quad (3)$$

where  $\delta = (2\pi\hbar^2/m_e k_B T)^{1/2}$  is the electron thermal de Broglie wavelength. For values of  $r \gg \delta$  the potential becomes Coulomb, while for  $r \ll \delta$  the Coulomb singularity is removed and  $V(r) \rightarrow -Ze^2/\delta + (Ze^2/2\delta^2)r$ . This is the simplest phenomenological form representing the short range effects of the uncertainty principle [16,17].

It is useful at this point to introduce dimensionless quantities. The length scale is chosen to be the average electron-electron distance  $r_0$ , defined in terms of the electron density  $n_e$  by  $4\pi n_e r_0^3/3 = 1$ . The dimensionless electron-electron and ion-electron potentials become

$$V_{ee}^*(r^*) = \beta V_{ee}(r) = \frac{\Gamma}{r^*},$$

$$V^*(r^*) = \beta V(r) = -\frac{Z\Gamma}{r^*} (1 - e^{-r^*/\delta^*}), \quad (4)$$

where  $r^* = r/r_0$ ,  $\delta^* = \delta/r_0$ , and  $\Gamma = \beta V_{ee}(r_0)$  is the usual electron coupling constant. In all of the following it is understood that dimensionless variables are used and the asterisk will be deleted for simplicity of notation.

The above describes the classical system to be studied. Since the electron-ion potential is bounded from below, it supports a stable equilibrium state whose properties have an intrinsic interest of their own. As discussed in the Introduction, the motivation for this system is an attempt to capture the most relevant features of an analogous quantum system. Accordingly, the regularization of the Coulomb potential is associated with the fact that an electron of thermal velocity cannot be localized at the ion in a volume smaller than  $\approx \delta^3$  due to the uncertainty principle [16,17]. More sophisticated forms obtained systematically from the two particle Slater sum are available [3–5], but the forms are qualitatively the same and the detailed differences are not important for the purposes here. To enforce this correlation with the quantum system further, it is useful to consider temperature and density conditions, for which classical trajectories might provide an approximate representation of the quantum dynamics. This cannot be made precise since there is no formal limit in which a classical Hamiltonian can be obtained from the quantum Hamiltonian due to the electron-ion interaction. Nevertheless, several qualitative limits can be identified. First, the localization of the electrons, characterized by their thermal de Broglie wavelength should be small compared to the average electron separation, i.e.,  $\delta < 1$ . Furthermore, most trajectories for the electron-ion interaction should occur for electron-ion distances that are large compared to the de Broglie wavelength. This can be quantified by requiring that the apse for  $90^\circ$  scattering should be larger than the de Broglie wavelength. The former is known as the Landau length and its size relative to the de Broglie wavelength is  $\sigma = Z\Gamma/\delta$ . This is also the maximum value of the electron-ion interaction in the reduced units assumed above,

$$|V(0)| = \frac{Z\Gamma}{\delta} = \sigma. \quad (5)$$

The classical condition  $\sigma > 1$  has two interesting and perhaps counterintuitive consequences. First, it implies that the strong electron-ion coupling is “more classical.” Also, since the Landau length is inversely proportional to the temperature, and the thermal de Broglie wavelength is inversely proportional to the square root of the temperature,  $\sigma > 1$  occurs at lower temperatures. Together with  $\delta$  this also implies lower densities. Figure 1 shows the density temperature plane illustrating two points with  $\sigma = 2.5Z$  and  $0.25Z$ . Figure 1 also provides a schematic of the current domains of experimental studies, mainly spectroscopic.

The existence of finite populations for ions of given  $Z$  depends on the temperature and density. If the ion is only partially ionized, the bound electrons should be treated quantum mechanically for an effective charge distribution at very

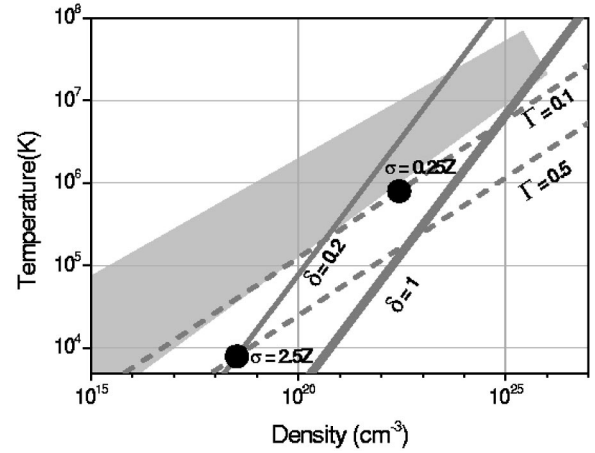


FIG. 1. Temperature-density plane showing state conditions studied here (solid circles). Also shown in gray scale is the laboratory plasma spectroscopy domain.

short distances, while the residual electrons interact with the resulting reduced nuclear charge via the regularized potential (3). For large net ionic charge, higher temperatures and higher densities are required. At fixed  $\delta < 1$ , Fig. 1 shows this implies more weakly coupled electrons (e.g.,  $n = 10^{25}$ ,  $T = 4.6 \times 10^7$  corresponds to  $\delta = 0.4$  and  $\Gamma = 1.4 \times 10^{-2}$ ). The reason for the lower temperatures and densities selected for the initial studies here is that MD simulation is more efficient at higher  $\Gamma$ . The price for this is that states supported by the classical model for larger  $Z$  values no longer have real quantum counterparts (equilibrium populations) at the lowest temperatures considered. Thus, the strongest coupling cases studied below are purely an exploration of the statistical mechanics for the classical model system under extreme conditions. The  $n, T, Z$  domain for physical relevance depends on the experiment and in some cases is larger than that determined from average equilibrium ionization values (e.g., spectroscopic studies of trace populations and nonequilibrium states in stopping power experiments). The study here essentially defines the limits on the parameter space for application of classical statistical mechanics for the attractive potential in Eq. (3). Application of these methods to high  $Z$  radiators under realistic inertial confinement fusion conditions will be given elsewhere.

### A. MD simulation

A primary motivation for associating the classical Hamiltonian (2) with the underlying quantum system is to allow application of molecular dynamics simulation. In principle, MD accounts for all correlations and many-body effects for both static and dynamic properties of classical systems. Generally, it has been exceptionally useful for providing the benchmarks for testing theoretical methods. Primary constraints and limitations follow from the finite system size (particle number), which is determined in part by the force range, and the time interval required for accurate statistics. However, new difficulties are encountered for the attractive ion-electron force considered here when  $|F(0)| = \sigma/2\delta$  becomes large. Then electron trapping by the ion in metastable

states with large lifetimes can occur, requiring very long simulation times to obtain good statistics for properties, such as electric fields. To allow the most efficient MD simulations, periodic boundary conditions are used and the potential is screened at distances of the order of the system size. This screening is always much larger than the correlation length, so the results are essentially the same as would be obtained with an Ewald sum to correct for small finite system size. In many respects MD numerical simulation can be regarded as an experiment. Similar features such as noise, dependence on apparatus performances, etc., common for experiments must be taken into account for MD as well. In principle, MD results always can be improved, but there are practical limitations. Simulation results can be taken as reliable data provided a careful protocol has been followed. As already mentioned, standard MD techniques have been used here, but for unusual conditions. In addition to their own mutual interaction, the electrons are submitted to a finite spherically symmetric attractive force due to an ion of variable charge. Thus, equations of motions for particles are solved in a fixed nonuniform external field that tends to concentrate the electrons about the ion. Several points have to be controlled carefully. First, the accretion of the electrons around the ion has to be compensated by a large number of particles in the simulation volume in order to minimize the depletion that might result at large distances, particularly in the case of large  $Z$ . Second, the size of the simulation volume has to be large enough to ensure that the numerical model is a relevant representation for the long range Coulomb potential, and to minimize interaction with other ions duplicated through the periodic boundary conditions. Third, equilibrium conditions have to be reached in the presence of the attractive central force. These equilibrium conditions are fulfilled provided a careful setup for the particles in the simulation volume is carried out before sampling the system. Practically, times representing several crossing times of an average electron over the simulation volume are considered. During this time, fluctuations in the total energy of the system must be negligible. Limitations related to strong electron-ion attraction are imposed for this protocol. For small de Broglie wavelength, an electron with a low kinetic energy can stay trapped in the attractive central potential for times comparable to the simulation time. Such events are interpreted as a failure of the simulation model, and do not occur for the results reported below. Nevertheless, the charge density structure near the ion, represented by the density correlation function at small  $r$ , shows generally a noticeable noise representative of a more difficult sampling in this domain. Finally, it should be mentioned that when compared to an OCP simulation carried out for  $N$  particles, the present simulations of the charge structure around an impurity require a factor of  $N$  times longer to reach an equivalent level of statistical sampling.

### B. Theory

The structural properties of interest are the electron charge distribution and electron electric fields (forces) at the ion. For the theoretical predictions, approximations known to be successful for same sign charges are tested for their ap-

plicability to an attractive potential. There is no *a priori* assurance that this is the case, since the physical states sampled are quite different. For repulsive potentials close configurations are suppressed, while here they become strongly enhanced. As will be seen below, even the mathematical properties of some models are changed dramatically by this difference. The approximations considered are such that the properties can be calculated once the ion-electron and electron-electron equilibrium pair distribution functions  $g_{ie}(r)$  and  $g_{ee}(r)$  are known. These are determined from the HNC [18], specialized to this case of a single ion in the electron gas. In this case  $g_{ee}(r) \equiv 1 + h_{ee}(r)$  is the same as that for a classical jellium and is determined from the coupled pair of HNC equations (recall that dimensionless units are used)

$$h_{ee}(r) = c_{ee}(r) + \frac{3}{4\pi} \int d\mathbf{r}' c_{ee}(|\mathbf{r} - \mathbf{r}'|) h_{ee}(r'), \quad (6)$$

$$1 + h_{ee}(r) = \exp[-V_{ee}(r) + h_{ee}(r) - c_{ee}(r)]. \quad (7)$$

The first of these is the Ornstein-Zernicke equation defining the direct correlation function  $c_{ee}(r)$ , while the second equation defines the HNC approximation. The ion-electron distribution  $g_{ie}(r) \equiv 1 + h_{ie}(r)$  is determined from a similar pair of equations

$$h_{ie}(r) = c_{ie}(r) + \frac{3}{4\pi} \int d\mathbf{r}' c_{ee}(|\mathbf{r} - \mathbf{r}'|) h_{ie}(r'), \quad (8)$$

$$1 + h_{ie}(r) = \exp[-V(r) + h_{ie}(r) - c_{ie}(r)]. \quad (9)$$

These results can be obtained from the HNC equations for a binary mixture in the limit of low concentration for one of the species. The pair of Eqs. (6) and (7) are autonomous and can be solved for both  $g_{ee}(r)$  and  $c_{ee}(r)$ . With the latter known, Eqs. (8) and (9) can be solved for  $g_{ie}(r)$ . A new code has been written to solve these equations following the general scheme of Rogers [5], and tested for the jellium without the impurity ion and with a negative ion (repulsive interaction) over a wide range of values for  $\Gamma$  including very strong coupling. In contrast, the parameter space for solutions to Eqs. (8) and (9) with the positive ion considered here is restricted to approximately  $\sigma \leq 7.5$ . Beyond this value unphysical solutions are obtained, but it is not clear if this is a limitation of the HNC approximation or its numerical implementation here.

A related useful property for analysis is the probability density for the position of the electron nearest the ion (nearest neighbor distribution). This is calculated from the probability to find an electron at position  $\mathbf{r}$ , times the probability to find none of the other particles any closer

$$g_{nn}(r) = g_{ie}(r) \left[ 1 - \frac{3}{4\pi N_e} \int_0^r dr' g_{ie}(r') \right]^{N_e - 1} \\ \rightarrow g_{ie}(r) \exp \left[ -\frac{3}{4\pi} \int_0^r dr' g_{ie}(r') \right]. \quad (10)$$

This is not an exact result, since the probabilities for each electron are treated as independent. For the attractive potential considered here, the electron density at such short distances is strongly enhanced and additional correlations might be expected to be required for this distribution.

The electron electric field at the ion, due to all electrons, is obtained from the total regularized potential (8)

$$\mathbf{E} = -\nabla_0 V(\{r_{i0}\}) = \sum_{i=1}^N \mathbf{e}(r_{i0}), \quad (11)$$

where  $\mathbf{r}_{i0} = \mathbf{r}_i - \mathbf{r}_0$  is the position of the  $i$ th electron relative to the ion, and

$$V(\{r_{i0}\}) = \sum_{i=1}^N V(r_{i0}), \quad \mathbf{e}(r_{i0}) = \frac{\hat{\mathbf{r}}_{i0}}{r_{i0}^2} \left[ 1 - \left( 1 + \frac{r_{i0}}{\delta} \right) e^{-r_{i0}/\delta} \right]. \quad (12)$$

The potential energy in the classical Gibbs ensemble is related to this potential by  $\beta U(\{r_{i0}\}) = Z\Gamma V(\{r_{i0}\})$ . This allows the (dimensionless) covariance of the electric field to be written in the form

$$\begin{aligned} C^* &= \frac{r_0^4}{e^2} \langle \mathbf{E} \cdot \mathbf{E} \rangle = -\frac{1}{Z\Gamma} \langle \nabla_0 \cdot \mathbf{E} \rangle \\ &= \frac{3}{4\pi Z\Gamma} \int d\mathbf{r} g_{ie}(r) \nabla \cdot \mathbf{e}(\mathbf{r}). \end{aligned} \quad (13)$$

Thus, the field covariance is completely determined from the electron charge density. A closely related quantity is the root mean square electron-ion force.

The probability density for electric field magnitudes (microfield distribution) is defined by

$$\begin{aligned} P(\epsilon) &= 4\pi\epsilon^2 \langle \delta(\boldsymbol{\epsilon} - \mathbf{E}) \rangle = \frac{\epsilon^2}{2\pi^2} \int d\boldsymbol{\lambda} e^{-i\boldsymbol{\lambda} \cdot \boldsymbol{\epsilon}} \langle e^{-i\boldsymbol{\lambda} \cdot \mathbf{E}} \rangle \\ &\equiv \frac{\epsilon^2}{2\pi^2} \int d\boldsymbol{\lambda} e^{-i\boldsymbol{\lambda} \cdot \boldsymbol{\epsilon}} e^{G(\boldsymbol{\lambda})}. \end{aligned} \quad (14)$$

The second equality defines the generating function  $G(\boldsymbol{\lambda})$ . In general, it is not fully determined from the charge density  $g_{ie}(r)$ . Instead, it has a formal representation as a series in correlations among the electrons and ion of all orders [19]

$$G(\boldsymbol{\lambda}) = \sum_{\ell=1}^N \int d\mathbf{r}_1 \cdots d\mathbf{r}_\ell g^\ell(\mathbf{r}_1 \cdots \mathbf{r}_\ell) \phi(\boldsymbol{\lambda}, \mathbf{r}_1) \cdots \phi(\boldsymbol{\lambda}, \mathbf{r}_\ell) \quad (15)$$

$$\phi(\boldsymbol{\lambda}, \mathbf{r}) = e^{i\boldsymbol{\lambda} \cdot \mathbf{e}(\mathbf{r})} - 1. \quad (16)$$

Here,  $g^\ell(\mathbf{r}_1 \cdots \mathbf{r}_\ell)$  is a cluster function representing the correlations among  $\ell$  electrons and the ion. In particular  $g^1(\mathbf{r}_1) = 3g_{ie}(r)/4\pi$ . At weak electron coupling it is expected that the series can be truncated at  $\ell=1$ , leading to the Baranger-Moser (BM) approximation [14]

$$P(\epsilon) = \frac{\epsilon^2}{2\pi^2} \int d\boldsymbol{\lambda} e^{-i\boldsymbol{\lambda} \cdot \boldsymbol{\epsilon}} \exp\left( \frac{3}{4\pi} \int d\mathbf{r} g_{ie}(r) \phi(\boldsymbol{\lambda}, \mathbf{r}) \right). \quad (17)$$

Consequently, in this approximation the microfield distribution is determined from the electron charge density alone. It is easily verified that the covariance of the microfield distribution calculated from the BM approximation differs from the exact result (13)

$$C^{BM} = \frac{3}{4\pi} \int d\mathbf{r} g_{ie}(r) \mathbf{e}(\mathbf{r}) \cdot \mathbf{e}(\mathbf{r}). \quad (18)$$

To account for multielectron correlations it is necessary to include higher order terms in the series of Eq. (15). An improvement on the BM microfield distribution is given by the APEX approximation [15]. This approximation can be obtained by defining a function  $\phi^*(\boldsymbol{\lambda}, \mathbf{r})$  in terms of a ‘‘renormalized field’’  $\mathbf{e}^*(\mathbf{r})$  [20]

$$\phi^*(\boldsymbol{\lambda}, \mathbf{r}) = e^{i\boldsymbol{\lambda} \cdot \mathbf{e}^*(\mathbf{r})} - 1. \quad (19)$$

It is straightforward to express  $\phi(\boldsymbol{\lambda}, \mathbf{r})$  in terms of  $\phi^*(\boldsymbol{\lambda}, \mathbf{r})$  and the ratio of field magnitudes  $R(r) = e(r)/e^*(r)$ ,

$$1 + \phi = (1 + \phi^*)^R. \quad (20)$$

Substitution of  $\phi$  as a function of  $\phi^*$  into the series (15) gives an equivalent series rearranged as a functional power series in  $\phi^*$ . Truncation of this series at  $\ell=1$  gives

$$G^{APEX} = \frac{3}{4\pi} \int d\mathbf{r} g_{ie}(r) R(r) \phi^*(\boldsymbol{\lambda}, \mathbf{r}). \quad (21)$$

The microfield distribution in this approximation is known as APEX and, like the Baranger-Moser approximation is specified entirely in terms of the electron charge density. The corresponding covariance is

$$C^{APEX} = \frac{3}{4\pi} \int d\mathbf{r} g_{ie}(r) \mathbf{e}(\mathbf{r}) \cdot \mathbf{e}^*(\mathbf{r}). \quad (22)$$

The unspecified field  $\mathbf{e}^*(\mathbf{r})$  is now chosen such that the result (22) is exact,  $C^{APEX} = C$ . It is anticipated that this enforcement of the exact covariance improves the overall microfield distribution as well. There are many ways in which this choice can be made, as discussed more completely below.

The distribution of microfields due to the nearest electron can be obtained from the nearest neighbor distribution (8). The magnitude of the electric field  $e(r)$  is inverted to find  $r(\epsilon)$  and the associated nearest neighbor probability distribution is defined by

$$P_{nn}(\epsilon) = \frac{dr(\epsilon)}{d\epsilon} 4\pi r^2(\epsilon) g_{nn}(r[\epsilon]). \quad (23)$$

Corrections to this approximation are discussed in [21].

In summary, the theoretical tools to be tested are the HNC integral equation for the charge density, the field covariance

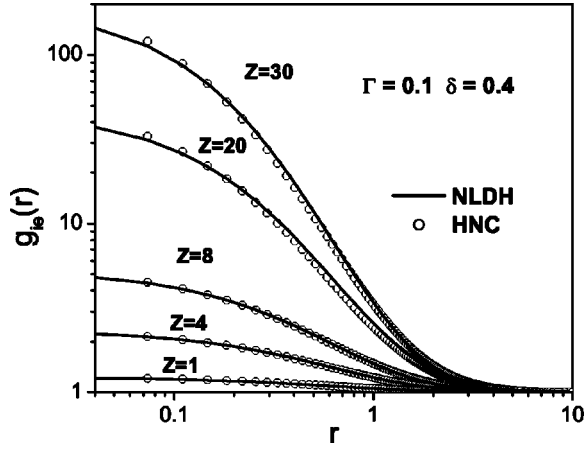


FIG. 2. Comparison of the nonlinear Debye-Hückel form for  $g_{ie}(r)$  with HNC for the high temperature case at  $Z=1, 4, 8, 20,$  and  $30$ .  $r$  is the dimensionless distance used all along the text.

derived from the charge density, and approximate models of the microfield distribution function expressed in terms of the charge density.

### III. CHARGE DENSITY

The quantity  $g_{ie}(r) = n_e(r)/n_e$  is the number density for electrons at a distance  $r$  from the ion, relative to its uniform value for  $Z=0$ . Since the potential is attractive this is expected to be an increasing function of  $r$  as  $r \rightarrow 0$ , and should approach unity as  $r \rightarrow \infty$ . Also,  $g_{ie}(0)$  should be finite due to the regularization of the Coulomb potential. To have an estimate of its dependence on the parameters  $Z, \Gamma,$  and  $\delta$  first eliminate  $c_{ie}(r)$  between Eqs. (8) and (9) to get the single equivalent equation

$$\ln[1 + h_{ie}(r)] = -V(r) + \frac{3}{4\pi} \int d\mathbf{r}' c_{ee}(|\mathbf{r} - \mathbf{r}'|) h_{ie}(r'). \quad (24)$$

Interestingly, this nonlinear equation for  $h_{ie}(r)$  is the same as that for the stationary solution to the nonlinear Vlasov equation. The only difference is that  $c_{ee}(r)$  is replaced in the latter by its weak coupling limit  $-\Gamma V_{ee}(r)$ . Thus the HNC equations for  $h_{ie}(r)$  have the same “physics” as the Vlasov equation, except with a renormalized electron-electron potential  $V_{ee}(r) \rightarrow -c_{ee}(r)/\Gamma$ . In fact, the weak electron-electron coupling is a good approximation for the conditions considered here so effectively we are studying ion-electron coupling via the Vlasov equation [it appears the pair of Eqs. (6) and (7) are a better representation for numerical purposes since the former is nonlocal but linear, while the latter is nonlinear but local]. Now consider the further limit of weakly coupled ion-electron interactions,  $\sigma \ll 1$ , so that  $h_{ie}(r) \ll 1$ . The linear approximation to Eq. (24) for weak coupling becomes

$$h_{ie}(r) = -V(r) - \frac{3\Gamma}{4\pi} \int d\mathbf{r}' |\mathbf{r} - \mathbf{r}'|^{-1} h_{ie}(r') \quad (25)$$

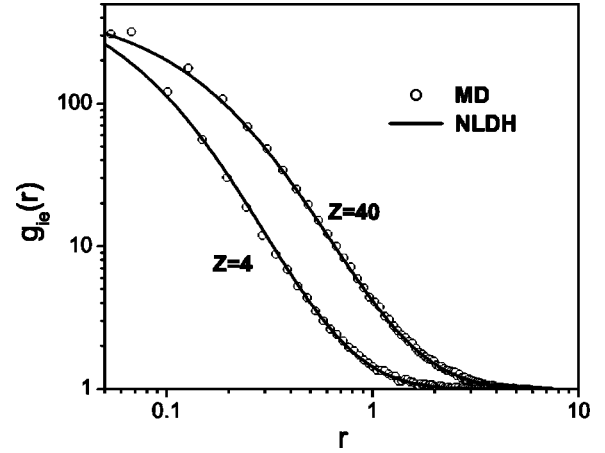


FIG. 3. Comparison of the nonlinear Debye-Hückel form for  $g_{ie}(r)$  with MD at  $\sigma=10$  ( $\Gamma=0.1, \delta=0.4, Z=40$  and  $\Gamma=0.5, \delta=0.2, Z=4$ ).

with the solution

$$g_{ie}(r) \approx 1 + \frac{Z\Gamma}{[1 - (\delta/\lambda)^2]} \frac{1}{r} (e^{-r/\lambda} - e^{-r/\delta}) \approx \exp\left(\frac{\bar{Z}\Gamma}{[1 - (\delta/\bar{\lambda})^2]} \frac{1}{r} (e^{-r/\bar{\lambda}} - e^{-r/\delta})\right). \quad (26)$$

The first line of Eq. (26) is the expected linear Debye-Hückel result for this regularized Coulomb potential, showing exponential screening for  $r > \lambda = 1/\sqrt{3\Gamma}$ . The *ad hoc* exponentiation on the second line is called the *nonlinear* Debye-Hückel approximation, and is an attempt to extend the linear form to stronger coupling. In addition the charge number and screening length have been replaced by  $\bar{Z}$  and  $\bar{\lambda}$  to account for possible form-preserving changes due to strong coupling. While there is no basis for Eq. (26) in theory, it is found to provide a useful quantitative reference description.

Figure 2 shows a fit of the nonlinear Debye-Hückel form to the solution to the HNC equation for the high density, high

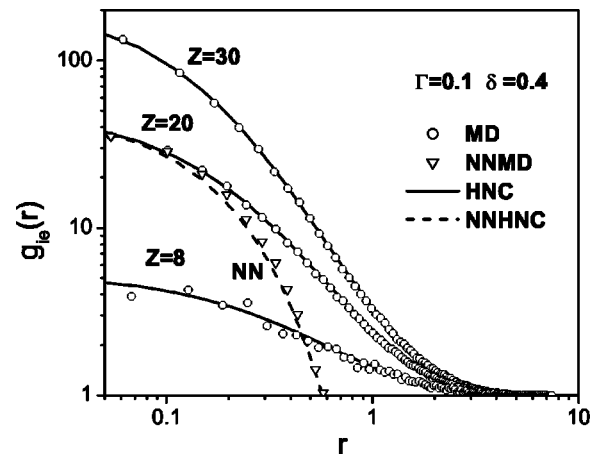


FIG. 4. Comparison of  $g_{ie}(r)$  from MD with that from HNC for  $Z=8, 20,$  and  $30$ . Also shown is the nearest neighbor result for  $Z=20$ .

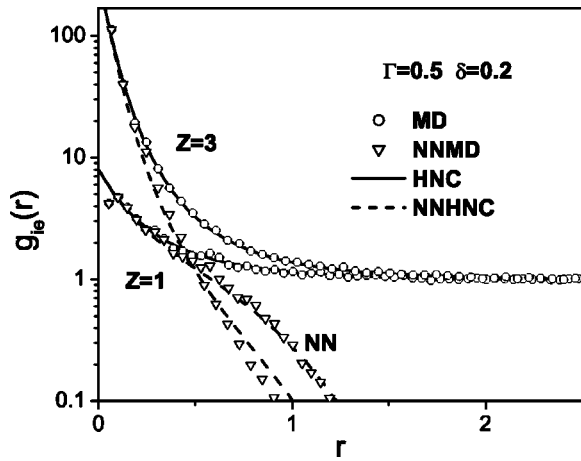


FIG. 5. Comparison of  $g_{ie}(r)$  from MD with that from HNC for  $Z=1$  and 3. Also shown are the nearest neighbor densities.

temperature case in Fig. 1, for  $Z=1, 4, 8, 20,$  and 30. The corresponding fit for the low density, low temperature case at  $Z=1$  and 3 is equally good. Comparisons at larger values of  $Z$  in each case could not be made since only unphysical solutions to the HNC equations could be obtained at these strong coupling values,  $\sigma > 7.5$ . However, it appears that the nonlinear Debye-Hückel form continues to be a good representation of the charge density as deduced from a fitting of the MD results. This is illustrated in Fig. 3 for  $Z=40$  at high temperature and  $Z=4$  at low temperature, both at  $\sigma=10$ .

The accuracy of the HNC calculations is tested in Figs. 4 and 5. The agreement is quite good in all cases. Also shown on these figures is the corresponding nearest neighbor distribution for the cases  $Z=1, 3,$  and 20. Discrepancies in the nearest neighbor distribution are expected even when the HNC  $g_{ie}(r)$  is accurate since the result (10) entails additional approximations beyond HNC [22]. These results illustrate the domain for which a single electron dominates the charge structure. The dominance of the nearest neighbor is characteristic of the conditions for all the discrepancies between the theory and MD simulation results observed in this work. It appears that generally the theoretical many-body approximations extend to attractive potentials, except

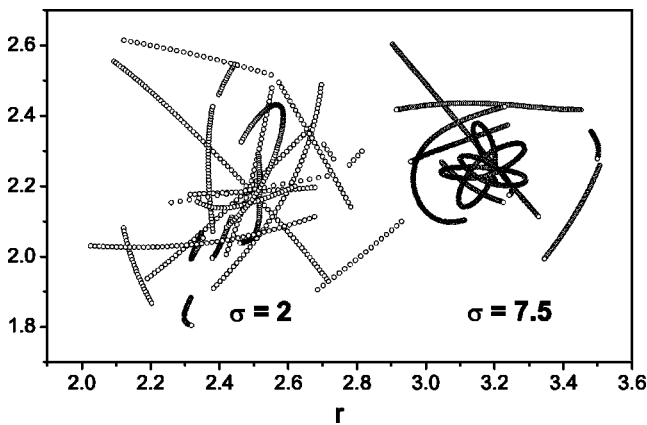


FIG. 6. Nearest neighbor trajectory plane projections for  $\sigma=2$  and  $\sigma=7.5$ .

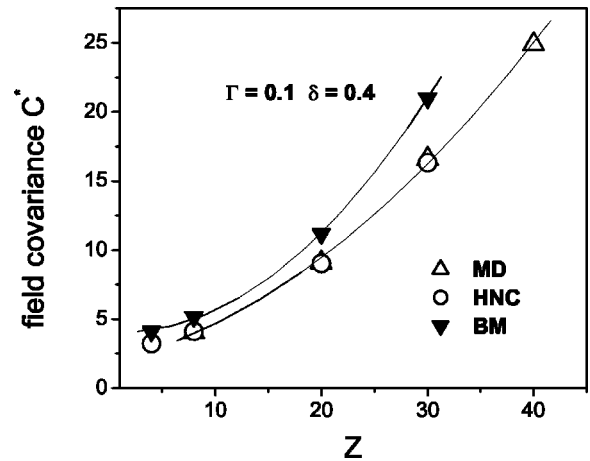


FIG. 7. Covariance  $C^*$  as a function of  $Z$  for the high temperature case; the solid lines are a quadratic fit to the data.

when a single perturber gives the dominant contribution. Figure 6 illustrates the qualitative differences between nearest neighbor trajectories for  $\sigma=2$  and  $\sigma=7.5$ . In the former case the domain of nearest neighbor trajectories is larger and many different particles become the nearest neighbor over the observation time. In contrast, at strong coupling the nearest neighbor lifetime is longer and the trajectory is much closer to the ion. Nevertheless, even for the strong coupling cases studied the lifetime of the nearest neighbor is small compared to the simulation time, as required by the protocol.

IV. ELECTRIC MICROFIELDS

For a first analysis of electron electric fields at the ion it is instructive to compare the evaluation of the covariance from the exact representation (13) using  $g_{ie}(r)$  from MD simulation and from HNC, as a measure of the importance of short range structure. Figures 7 and 8 show the dimensionless covariance  $C^*$  as a function of  $Z$  for the high density, high temperature and low density, low temperature cases, respectively. Also shown is the BM approximation form (18) calculated with  $g_{ie}(r)$  from HNC, and the solid lines are a fit of

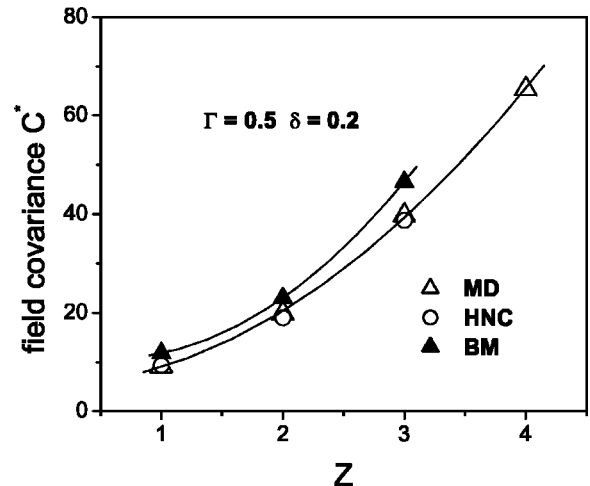


FIG. 8. Same as Fig. 7 for the low temperature case.

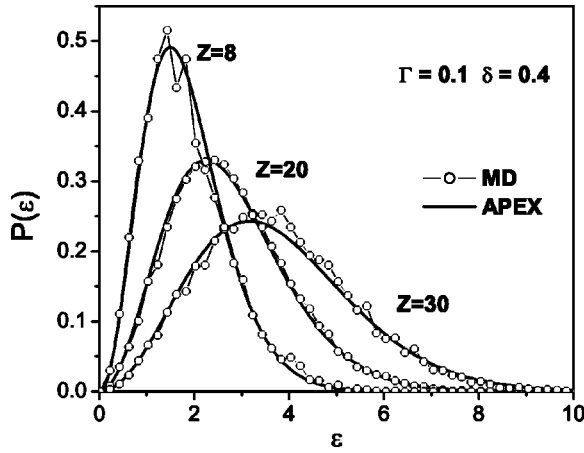


FIG. 9. Comparison of microfield distributions from MD and APEX for the high temperature case. A dimensionless microfield in units of  $e/r_0^2$  is used.

the data to a quadratic form in  $Z$ . In both cases it is seen that the exact form (13) yields the same results using either HNC or MD, as expected from the good agreement for  $g_{ie}(r)$ . In the low temperature case HNC does not converge for  $Z > 3$  so only the MD result is shown for  $Z=4$ . The trends are the same in the two cases, with increased covariance at larger  $Z$ , as expected from the enhanced charge density at smaller distances from the ion. The Baranger-Moser approximation shows significant deviation from the exact form, indicating that the microfield distribution in this approximation may show similar differences from the MD results.

The microfield distributions from MD and APEX are compared in Fig. 9 for the high temperature case at  $Z=8, 20$ , and  $30$  corresponding to the coupling values of  $\sigma=2, 5$ , and  $7.5$ . It is seen that APEX gives a quite good approximation even at the strongest coupling values (the case  $Z=40$ , not shown for clarity of the figure, shows a similar good agreement between APEX and MD). The same results are shown in Figs. 10–12, including the BM approximation and the corresponding nearest neighbor distributions. In all cases, the

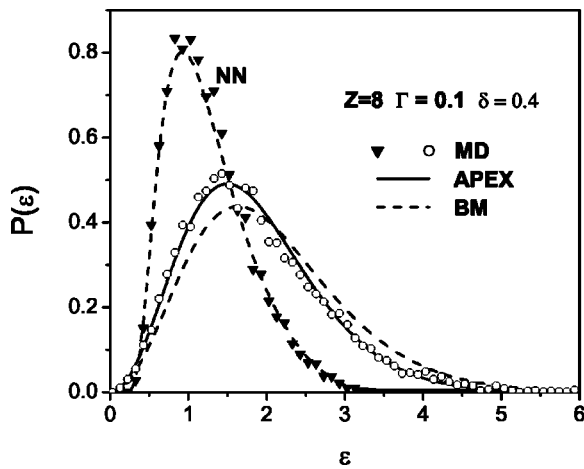


FIG. 10. Comparison of microfield distributions from MD, BM, and APEX for  $Z=8$ , for the high temperature case. Also shown is the nearest neighbor microfield distribution from MD.

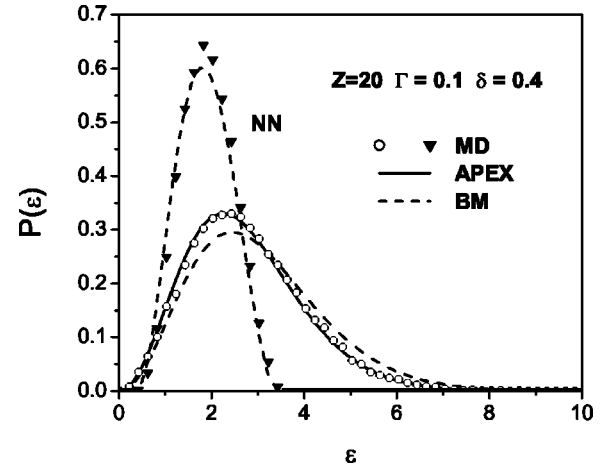


FIG. 11. Same as Fig. 10 for  $Z=20$ .

microfield distribution differs significantly from the nearest neighbor distribution, showing that collective electron effects dominate. The nearest neighbor distribution vanishes for fields greater than the largest single particle field,  $|e(0)| \approx \sigma/2\delta$ . Also, in all cases APEX is a significant improvement upon BM although the latter is qualitatively correct. This is expected from the behavior of the covariance in Fig. 7.

Now consider the low temperature case. Figures 13–15 show a comparison of MD, APEX, and BM for  $Z=1, 3$ , and  $4$  corresponding to the coupling values of  $\sigma=2.5, 7.5$ , and  $10$ . In contrast to the high temperature case, the nearest neighbor distribution becomes more similar to the full distribution as the coupling strength is increased. This shows the increasing dominance of the nearest neighbor. As this occurs, there is a qualitative change in the shape of the microfield distribution with the appearance of a shoulder and broadening around the most probable value. Interestingly, the Baranger-Moser approximation shows these general new features, and APEX provides corrections for a good quantitative representation except at the strongest coupling case. In the latter, the MD result for the nearest neighbor distribution is almost indistinguishable from that for the full distribution.

The APEX calculation has been performed in two ways, corresponding to two different choices for the renormalized

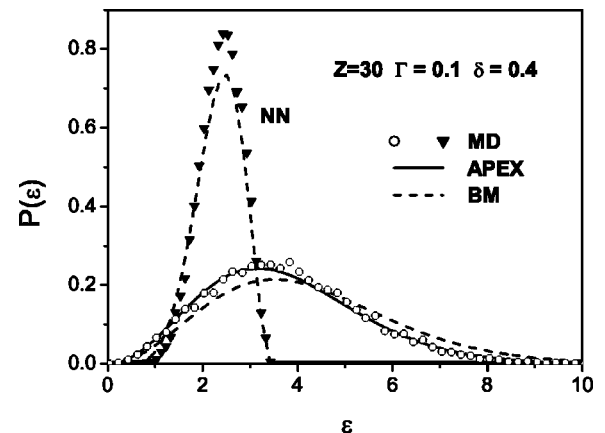


FIG. 12. Same as Fig. 10 for  $Z=30$ .

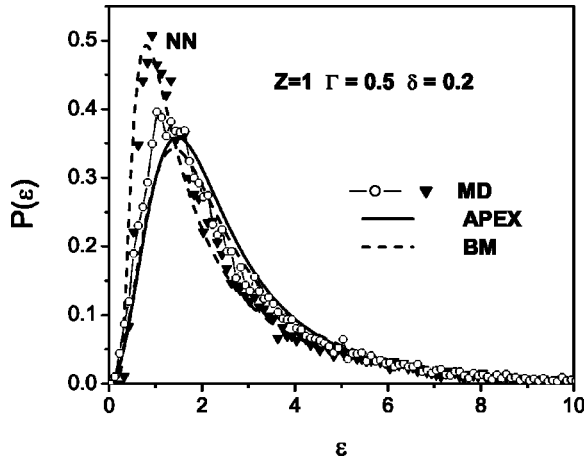


FIG. 13. Comparison of microfield distributions from MD, BM, and APEX for  $Z=1$ , for the low temperature case. Also shown is the nearest neighbor microfield distribution from MD and BM.

field  $e^*$ . In general, this effective single particle field is chosen to represent the average effects of correlations through some adjustable parameters that are chosen to impose the correct covariance through Eq. (22). To suggest some possibilities, consider the field derived from the potential of mean force

$$e^*(r) = \ln g_{ie}(r) \\ \approx \nabla \frac{\bar{Z}}{Z} \frac{1}{[1 - (\delta/\bar{\lambda})^2]} \frac{1}{r} (e^{-r/\bar{\lambda}} - e^{-r/\delta}),$$

where the second line follows using the nonlinear Debye approximation. This effective field has two effects due to correlations, a long range screening through the parameter  $\bar{\lambda}$ , and an overall intensity change through the effective charge number  $\bar{Z}$ . For same sign perturbors the correlations are long range and the standard method is to vary  $\bar{\lambda}$  with  $\bar{Z}=Z$  introduced and adjusted to enforce the correct covariance. In the case of the attractive force here the effective charge number  $\bar{Z}$  is used to require the correct covariance, with  $\bar{\lambda}$  con-

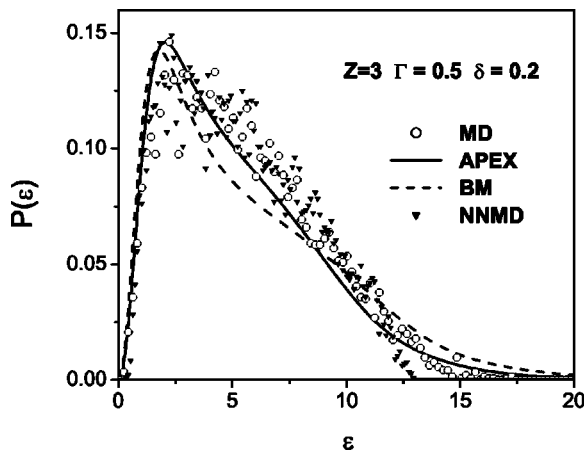


FIG. 14. Same as Fig. 13 for  $Z=3$ .

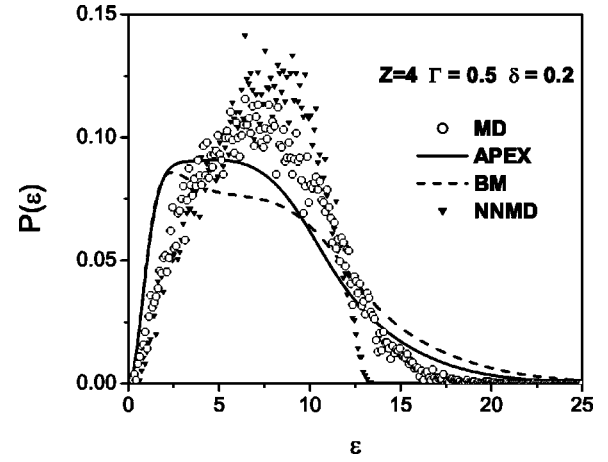


FIG. 15. Same as Fig. 13 for  $Z=4$ .

stant and of the order of the system size. This appears to represent better the short range correlations, particularly at stronger electron-ion coupling. As  $\sigma$  increases, the second method becomes more accurate and the first tends to fail. The figures presented here for APEX are based on adjusting  $\bar{Z}$ .

## V. DISCUSSION

The objective here has been to explore in detail the application of MD and selected many-body methods to describe the electron charge density and electric fields in the vicinity of a positive ion. A model classical system has been postulated based on a regularized Coulomb potential at short distances. Attention has been focused on the applicability of MD and the theory at strong electron-ion coupling, to explore the qualitative differences arising from a strongly attractive potential.

One measure of the coupling between the electrons and the ion is the value of the potential at the ion,  $\sigma = Z\Gamma/\delta$ . Another is the corresponding value for the force,  $\sigma/2\delta$ . The studies here were limited to  $\sigma \leq 10$ . At the highest values the charge density increases by two orders of magnitude near the ion, and the HNC integral equations fail to yield physically meaningful solutions. MD simulation continues to be effective at these strong coupling values, but further increase leads to difficulties discussed above (e.g., the persistence of a trapped electron near the ion). Such conditions are likely to be only of academic interest for the model classical system, with no corresponding quantum counterpart. For  $\sigma \leq 5$  the solutions obtained from HNC agree well with those from MD. This may be surprising at first since the HNC equations were originally obtained for repulsive potentials, whose solutions are qualitatively different from those presented here. One possible explanation for its applicability here is the close relationship of the HNC equations to the nonlinear Vlasov equation for weakly coupled electrons. The Vlasov equation has a clear physical meaning as a mean field limit, even for strong electron-ion coupling. For the conditions considered here the HNC equations are practically equivalent to the Vlasov equation. Interestingly, the form of the solution ob-

tained for weak electron-ion coupling persists at strong coupling by simple exponentiation and renormalization of the charge number and screening length (the nonlinear Debye-Hückel form). This representation is found to fit the MD results as well at the strongest coupling values, for which no solution to the HNC equations could be obtained. This suggests that other means to solve the equation may be more appropriate for strong coupling, such as variational methods based on the nonlinear Debye-Hückel form.

The electric field of the electrons at the ion is finite since it is derived from the regularized Coulomb potential. Consequently, a single electron can contribute no more than  $\sigma/2\delta$ . In contrast to fields around an ion of the same sign charge, the largest fields in this case are due to collective many-body effects. Since the electric field is largest for close configurations, and these are enhanced by the attractive potential, the sampling in MD simulation requires more care than in the same sign case. An average value for the field can be defined as the root mean square of the covariance,  $\bar{\epsilon} \equiv \sqrt{C^*}$ . Figures 7 and 8 show that this average value increases with  $Z$  due to the increased accumulation of charge at short distances. The BM covariance (18) differs from the exact result (13) by terms depending on the correlation of two electrons in the presence of the ion. For a repulsive potential these correlations affect the screening at distances of the order of the Debye length. Here, these additional correlations occur primarily at short distances and behave as an additional screening of the ionic charge. This is deduced from the fact that enforcement of the exact covariance in APEX is improved if the renormalized field  $e^*(r)$  is defined in terms of an effective ion charge rather than an effective screening length.

The microfield distributions calculated in this way from APEX are in very good agreement with those from MD simulation for all charge numbers in the high temperature case. This includes the extreme coupling of  $\sigma=10$  at  $Z=40$ . The BM approximation is qualitatively correct but only semiquantitative. Again, it is somewhat surprising that these approximations derived for repulsive potentials are so good for these physically opposite conditions. For increasing  $Z$  the peak shifts and broadens to emphasize higher field values. A characteristic of this high temperature case is a qualitatively different nearest neighbor distribution, which misses most of the distribution above the peak value. This indicates that the closest electron, with the largest single electron field, is dominated by the collective coherent fields of many particles. This effect actually increases at stronger couplings.

In contrast, the microfield distributions for the lower temperature case have an opposite trend. As the electron-ion coupling increases the nearest neighbor distribution becomes closer to that of the full distribution. In Figs. 14 and 15 the two distributions can be distinguished only at the largest field values. In addition, the shape of the full distribution becomes distorted in the direction of the nearest neighbor form. This entails a shift of the peak, as required by the covariance, but also a tendency to enhance the distribution for field values below the maximum of the nearest neighbor distribution. The BM and APEX approximations reproduce these trends, but they no longer provide quantitative accuracy at strong couplings.

This difference between the high and low temperature cases cannot be explained in terms of the coupling parameter  $\sigma$ . Instead, it is more likely that the maximum force parameter  $\sigma/2\delta$  represents the difference. The two examples of Fig. 3 have the same value of  $\sigma=10$ , but  $\sigma/2\delta$  for the low temperature case is twice that of the high temperature case. This is probably the reason for nearest neighbor dominance in this case, with increasing lifetime for each nearest neighbor as the maximum force increases. These effects are even more evident for dynamical properties. Elsewhere it will be shown that the electric field time correlation function is well approximated by the single particle dynamics of the nearest neighbor electron in the low temperature case.

## VI. CONCLUSION

Both MD and current theoretical methods developed for repulsive potentials have been shown to apply as well for the attractive classical electron-ion system. The accuracy of these methods extends even to strong attraction where electron densities increase by several orders of magnitude. These results justify application of these methods to more practical conditions of experimental interest. These include the low  $Z$  ions produced at low temperatures by short pulse lasers, and the high  $Z$  ions for diagnostics in hot, dense laser fusion plasmas.

The primary results of this study can be summarized as follows.

(1) The electron charge density and electron electric fields at the ion can be studied efficiently and accurately by MD simulation, even at strong electron-ion coupling, except for conditions where close electron-ion configurations begin to become important. The latter occurs primarily for the low temperature case ( $\Gamma=0.5, \delta=0.2$ ). In this domain, changes in the implementation of APEX are required for the microfield distribution.

(2) The HNC solution is reasonably well approximated by the nonlinear Debye distribution, with an effective charge number and screening length.

(3) MD is effective for simulation of the charge density and electron electric fields as well, although the lifetime of electrons close to the ion increases for stronger couplings. Such short range single electron dynamics leads to large electric fields and requires better statistics to ascertain their relative contribution to ensemble averages. Discrepancies between the MD results and theory for the charge densities at short distances increase at strong coupling differences. Furthermore, the HNC integral equations fail to converge for  $\sigma>7.5$ . Similarly, both BM and APEX show qualitative as well as quantitative differences from the MD results whenever the nearest neighbor field becomes important.

## ACKNOWLEDGMENTS

Support for this research has been provided by the U.S. Department of Energy Grant No. DE-FG03-98DP00218. J.D. is grateful to the University of Provence for its support and hospitality.

- [1] S. Ichimaru, *Statistical Plasma Physics, Frontiers in Physics* Vol. I (Addison-Wesley, New York, 1992), p. 87.
- [2] D. Brydges and Ph. Martin, *J. Stat. Phys.* **96**, 1163 (1999).
- [3] G. Kelbg, *Ann. Phys. (Leipzig)* **12**, 219 (1963); **13**, 354 (1964); **14**, 394 (1964).
- [4] W. Ebeling, *Ann. Phys. (Leipzig)* **19**, 104 (1967); W. Ebeling, B. Miltzer, and F. Schautz, *Contrib. Plasma Phys.* **37**, 137 (1997).
- [5] F.J. Rogers, *J. Chem. Phys.* **73**, 6272 (1980); *Phys. Rev. A* **29**, 868 (1984).
- [6] D. Klakow, Ch. Toepffer, and P.-G. Reinhard, *J. Chem. Phys.* **101**, 10 766 (1994); M. Knaup, P.-G. Reinhard, and Ch. Toepffer, *Contrib. Plasma Phys.* **39**, 57 (1999).
- [7] J.-P. Hansen and I.R. McDonald, *Phys. Rev. A* **23**, 2041 (1981).
- [8] G. Zwicknagel, C. Toepffer, and P.-G. Reinhard, *Phys. Rep.* **309**, 118 (1999).
- [9] T. Pschiwul and G. Zwicknagel, *Contrib. Plasma Phys.* **41**, 271 (2001).
- [10] J. Ortner, I. Valuev, and W. Ebeling, *Contrib. Plasma Phys.* **39**, 311 (1999).
- [11] B. Talin and J. Dufty, *Contrib. Plasma Phys.* **41**, 195 (2001).
- [12] B. Talin, A. Calisti, E. Dufour, and J. Dufty, *J. Quant. Spectrosc. Radiat. Transf.* **71**, 729 (2001).
- [13] B. Talin, A. Calisti, and J. Dufty, *Contrib. Plasma Phys.* **41**, 323 (2001).
- [14] M. Baranger and B. Mozer, *Phys. Rev.* **115**, 521 (1959); B. Mozer and M. Baranger, *ibid.* **118**, 626 (1960).
- [15] C.A. Iglesias and J. Lebowitz, *Phys. Rev. A* **27**, 2705 (1983).
- [16] T. Morita, *Prog. Theor. Phys.* **22**, 757 (1959).
- [17] H. Minoo, M.-M. Gombert, and C. Deutsch, *Phys. Rev. A* **23**, 924 (1981).
- [18] J.-P. Hansen and I. McDonald, *Theory of Simple Liquids* (Academic Press, San Diego, 1990).
- [19] J.W. Dufty, in *Strongly Coupled Plasmas*, Vol. 154 of *NATO Advanced Studies Institute, Series B: Physics*, edited by H. de Witt and F. Rogers (Plenum, New York, 1987).
- [20] J.W. Dufty, D.B. Boercker, and C.A. Iglesias, *Phys. Rev. A* **31**, 1681 (1985).
- [21] C.A. Iglesias, C.F. Hooper, and H.E. De Witt, *Phys. Rev. A* **28**, 361 (1983).
- [22] S. Ichimaru, S. Mitake, S. Tanaka, and X.-Z. Yan, *Phys. Rev. A* **32**, 1768 (1985); **32**, 1775 (1985).